Long-Term Evolution of Debris Clouds in Low Lunar Orbit

Nathan R. Boone*
Air Force Institute of Technology
Robert A. Bettinger†
Air Force Institute of Technology

ABSTRACT

Simulations of spacecraft breakup events in lunar orbit are conducted with the aim of determining the longevity of the resulting debris and the hazards it could pose. The trajectories of approximately 73,000 debris particles across six Monte Carlo breakup simulations are propagated using a high-precision lunar trajectory model. Debris was found to be especially long-lasting for breakups in circular polar orbits at 200 km altitude and in retrograde equatorial orbits at 100 km or higher, with the majority of the debris not decaying during the one-year simulation time window. Analysis of the locations at which polar-orbiting debris tended to impact the Moon reveals a surprising asymmetry and significant accumulations in certain regions. Finally, estimates of the collision probability over one year to other notional spacecraft varied from 10^{-9} to 10^{-13}, suggesting a low risk of collision, but a significant number of close approaches within 5 km were observed. The results of this study provide new insights into the overall behavior of debris in lunar orbit and improve understanding of the consequences of a debris event in this orbital environment.

1. INTRODUCTION

The past decade has witnessed increasing interest in lunar exploration, with space probes recently sent to the Moon by the United States, China, India, and Israel. The number of lunar space missions is likely to increase further in the coming years as plans for crewed lunar exploration begin to take shape, particularly through the NASA Artemis Program. A growing number of space missions operating in lunar orbit may require a new focus on avoiding the generation of space debris in this environment, much like the recent focus on space debris in orbits near Earth. These considerations would be especially important with renewed crewed exploration of the Moon.

The threats from Earth-orbiting debris are relatively well-understood, with studies demonstrating the importance of debris management to avoid a potential "Kessler Syndrome," in which an increasing density of debris causes a cascading series of collisions that renders certain orbits unusable [1]. There have been few prior studies of the risk from debris in lunar orbit. Johnson [2] suggested in 1999 that lunar debris could someday become a concern, recommending the development of guidelines for disposal of objects in lunar orbit in anticipation of increasing space missions to the Moon in the second half of the 21st century. Boone and Bettinger [3] simulated spacecraft breakups in a polar lunar orbit, finding that the debris was stable in lunar orbit for at least a month after the breakup events. The potential for remarkable longevity of objects in lunar orbit was recently demonstrated by Meador [4], who found that the Apollo 11 Lunar Module Ascent Stage could still remain in lunar orbit to this day, over 60 years later. Additional studies of the risks from lunar debris are necessary to determine if debris mitigation strategies will be required to prevent a long-term accumulation of debris in lunar orbit.

This study seeks to evaluate the threat of lunar debris by analyzing the consequences of a significant debris-generating event in terms of the longevity of the debris particles in lunar orbit, the distribution of lunar surface impacts, and the collision risk to other lunar spacecraft. Monte Carlo simulations were conducted for breakup events in polar lunar orbits, often used by lunar mapping spacecraft, and retrograde equatorial orbits, used historically by the Apollo spacecraft. For each orbit type, the rate at which particles decayed to the lunar surface over the following year after

*PhD Student, Air Force Institute of Technology, Department of Aeronautics & Astronautics, Wright-Patterson AFB, OH, 45433, United States (nathan.boone@afit.edu)

†PhD, Assistant Professor, Air Force Institute of Technology, Department of Aeronautics & Astronautics, Wright-Patterson AFB, OH, 45433, United States (robert.bettinger@afit.edu)

the breakup was determined, and the locations at which debris particles struck the Moon were mapped. Collision risk probabilities were also calculated for notional spacecraft operating in polar and retrograde equatorial lunar orbits. The findings of this study improve understanding of the consequences of breakup events in lunar orbit and help to evaluate the importance of avoiding these events in the future.

2. METHODOLOGY

This research effort required a high-precision lunar orbit propagator for modeling the trajectories of objects in lunar orbit, a model for the properties of particles released in a spacecraft breakup event, and a method for calculating the collision risk from the debris. These models, and the design of the Monte Carlo debris experiments, are discussed in the following sections.

2.1 High-Precision Lunar Orbit Propagator

A high-precision lunar orbit propagator was developed to model the motion of debris particles in lunar orbit. This propagator includes perturbations due to the non-spherical lunar gravity field, the point-mass gravity of the Earth and Sun, and the force due to solar radiation pressure. After summing all accelerations, the positions and velocities of particles were obtained through numerical integration using an explicit Runge-Kutta method of order 5(4). The model was validated by comparison to NASA's General Mission Analysis Tool (GMAT).

2.1.1 Coordinate Frames

Trajectories were numerically integrated in the selenocentric "Moon Inertial" frame. The Moon Inertial frame is a coordinate frame aligned with the Moon's equator and spin axis direction at the J2000 epoch. The x-axis points along the the intersection of the x-y plane of the International Cartesian Reference Frame (ICRF) and the Moon's equator at the J2000 epoch, the z-axis points along the Moon's spin axis at the J2000 epoch, and the y-axis completes the right-handed coordinate system. The constant rotation matrix from the Moon Inertial frame to the ICRF is, from [5]:

$$[ROT]^{ICRF}_{MoonInertial} = \begin{bmatrix} 0.998496505205088 & 4.993572939853833\times10^{-2} & -2.260867140418499\times10^{-2} \\ -5.481540926807404\times10^{-2} & 0.909610125238044 & -0.411830900942612 \\ 0.000000000000000 & 0.412451018902688 & 0.910979778593430 \end{bmatrix} \tag{1}$$

The lunar Principal Axis (PA) Frame was used as the Moon-fixed coordinate system for computing the acceleration due to lunar gravity. This coordinate frame is fixed to the principal axes of the Moon [6]. The rotation matrix from the ICRF to the PA Frame is a 3-1-3 rotation by the lunar libration angles ϕ, θ, and ψ [7]. The lunar libration angles may be obtained from the JPL DE421 ephemerides [8]. The rotation matrix from the ICRF to the PA Frame is:

$$\left[ROT\right]^{PA}_{ICRF} = \begin{bmatrix} \cos\psi\cos\phi - \sin\psi\cos\theta\sin\phi & \cos\psi\sin\phi + \sin\psi\cos\theta\cos\phi & \sin\psi\sin\theta \\ -\sin\psi\cos\phi - \cos\psi\cos\theta\sin\phi & -\sin\psi\sin\phi + \cos\psi\cos\theta\cos\phi & \cos\psi\sin\theta \\ \sin\theta\sin\phi & -\sin\theta\cos\phi & \cos\theta \end{bmatrix} \tag{2}$$

2.1.2 Lunar Gravity Model

The lunar gravitational acceleration was determined using the GRAIL GRGM 1200A spherical harmonic lunar gravity model [9], truncated to degree and order 100. A 100×100 gravity model was selected based on comparison with GMAT, as discussed in Section 2.1.5. Additionally, Song et al. [7] studied the decay of lunar orbiters with lifetimes of approximately 160 days, finding that a 50×50 gravity model was sufficient to precisely predict the time required to decay.

2.1.3 Gravity of Earth and Sun

The acceleration due to the point-mass gravity of the Earth and Sun was calculated by obtaining the relative position vectors to the Earth and Sun from the JPL DE421 ephemerides [8]. To avoid numerical issues related to the similar distances between the Moon and the Earth/Sun and the particles and the Earth/Sun, the $f(q)$ method described by

Battin [10] was employed. Once the $f(q)$ function has been calculated according to Section 8.3 of Ref. [10], the third-body disturbing acceleration $\vec{a}_{TB}$ is:

$$\vec{a}_{TB} = -\sum_{k=1}^{n} \frac{\mu_k}{d_k^3} (\vec{r} + f(q_k)\vec{s}_k) \tag{3}$$

where n is the number of disturbing bodies (two in this research), μ_k is the standard gravitational parameter of the k^{th} disturbing body, d_k is the distance from the particle to the k^{th} disturbing body, $\vec{s}_k$ is the vector from the Moon to the k^{th} disturbing body, $f(q_k)$ is the $f(q)$ function for the k^{th} disturbing body, and $\vec{r}$ is the particle position relative to the Moon.

2.1.4 Solar Radiation Pressure

The following model for the force due to solar radiation pressure was used [11][12]:

$$\vec{a}_{SR} = (1-\nu)\frac{p_{SR} c_R A_c}{m} \frac{\vec{r}_{sun}}{|\vec{r}_{sun}|} \tag{4}$$

where p_{SR} is the force of solar pressure ($4.56 \times 10^{-6} \mathrm{N/m^2}$), c_R is the coefficient of reflectivity and was assumed to be equal to 1.2, A_c is the known cross-sectional area of the object, m is the known mass of the object, $\vec{r}_{sun}$ is the vector from the sun to the object, and ν is the shadow function. The shadow function is zero in full sunlight, one in full eclipse, and a number between zero and one in partial eclipse. The shadow function was calculated according to the method described by Montenbruck [12] and in the GMAT documentation [5].

2.1.5 Model Validation

This study seeks to understand how long objects following a breakup would remain in lunar orbit, so the trajectory model must be able to accurately model the perilune of objects over time. Lunar orbits with identical initial conditions were simulated with both GMAT and the orbit propagator developed for this research, referred to as LunarProp, for validation. The orbit propagation using GMAT included a 360×360 lunar gravity model, the point-mass gravity of the Earth and Sun, and solar radiation pressure. The perilune was returned from both GMAT and LunarProp and compared.

Simulations of lunar polar and retrograde equatorial orbits at 100 km altitude were used as comparison cases. The gravity model degree and order and the integration tolerances used in LunarProp were adjusted based on this comparison to achieve an acceptable balance between computation time and accuracy. The use of gravity model degrees and orders beyond 100×100 had a minimal impact on the accuracy of the orbit propagation, so a 100×100 gravity model was used for all propagation in this research. Numerical integration tolerances of 1×10^{-7} relative and 1×10^{-9} absolute were chosen because they lead to perilunes that never differ from GMAT by more than 0.6 km for the polar case and 3.7 km for the retrograde equatorial case. At this accuracy level, the evolution of the perilune over time as determined by LunarProp is visually almost indistinguishable from GMAT, as shown in Fig. 1.

2.2 NASA Standard Breakup Model

The NASA Standard Breakup Model [13] was used to calculate the properties of the fragments generated by the lunar spacecraft breakup event. The NASA Standard Breakup Model is a statistical model based on empirical data that returns the mass, size, cross-sectional area, ejection velocity, and number of particles following a spacecraft fragmentation event. The number of particles of characteristic length L_c or greater (in meters) is given by the power law equation:

$$N(L_c) = 6L_c^{-\beta} \tag{5}$$

where β is a constant equal to 1.6. The power law is only validated down to particles that are at least 10 cm in size [13], so particles below this size were not considered. Particles larger than 10 cm would also be the most likely to cause significant damage to a spacecraft in a collision. According to Eq. (5), there should be approximately 238 particles of size 10 cm or larger.

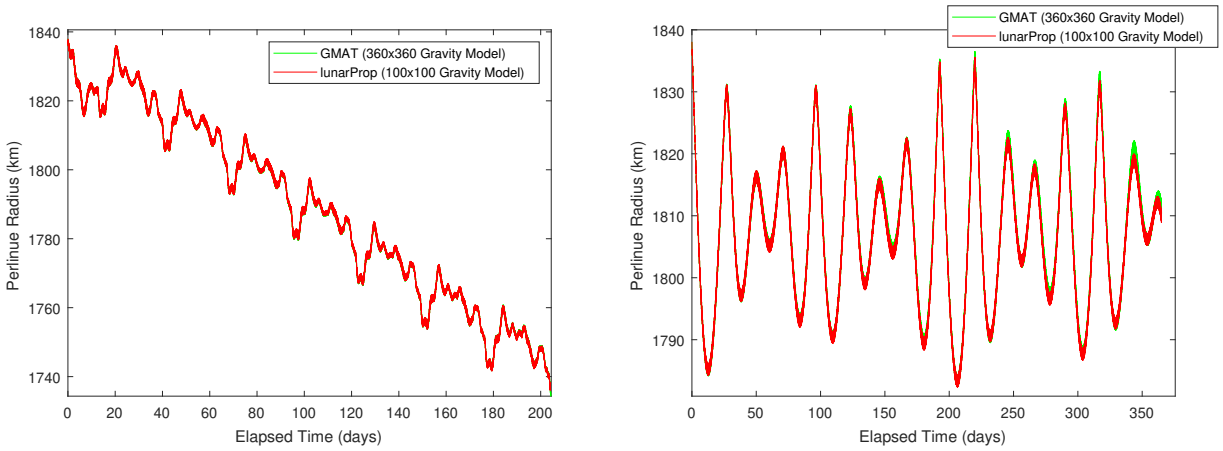

(a) 100 km Polar Lunar Orbit

(b) 100 km Retrograde Equatorial Lunar Orbit

Fig. 1: Comparison of Perilune Over Time for GMAT and LunarProp

Particle characteristic lengths were determined from this power law relationship using the following equation from Frey [14]:

$$\lambda = -\frac{1}{\beta}\log_{10}\left(10^{-\beta\lambda_0} - P_\lambda\left(10^{-\beta\lambda_0} - 10^{-\beta\lambda_1}\right)\right) \tag{6}$$

where P_λ is a random variable uniformly distributed between 0 and 1. λ, λ_0, and λ_1 are given by:

$$\lambda = \log_{10}(L_c) \tag{7}$$

$$\lambda_0 = \log_{10}(L_{c_0}) \tag{8}$$

$$\lambda_1 = \log_{10}(L_{c_1}) \tag{9}$$

where L_{c_0} is the lower particle size limit of 10 cm and L_{c_1} is the upper boundary on the characteristic length. The upper boundary was assumed to be 1 m based on the recommendation of Krisko [15], who indicates that the power law may break down for sizes above 1 m.

After randomly determining a particle characteristic length using Eq. (6), the distribution functions provided by Johnson [13] were used to randomly generate the area-to-mass ratio and the ejection velocity. Only the magnitude of the ejection velocity is provided by the breakup model, but a direction can be assigned by assuming an omnidirectional explosion and picking a random direction for the ΔV [16]:

$$\Delta V_x = \Delta V\sqrt{1-u^2}\cos\theta \tag{10}$$

$$\Delta V_y = \Delta V\sqrt{1-u^2}\sin\theta \tag{11}$$

$$\Delta V_z = \Delta V u \tag{12}$$

where u is a random number uniformly sampled between -1 and 1 and θ is a random angle uniformly sampled between 0 and 2π. The velocity vectors generated by one run of the breakup model are plotted in Fig. 2.

Generating the number of particles specified by Eq. (5) will generally lead to too little mass relative to the original pre-explosion mass of the spacecraft. Krisko [15] recommends to enforce mass conservation by generating two to eight additional fragments larger than 1 m that comprise the majority of the fragment mass. These objects would represent larger components not totally destroyed in the explosion, such as pressurant tanks, nozzle bells, etc. Therefore, up to eight additional fragments in the characteristic length range $L_{c_0} = 1$ and $L_{c_1} = 5$ were randomly generated until the total fragment mass matched the assumed pre-explosion mass of the spacecraft to within a tolerance of 5%. The pre-explosion mass of the spacecraft was assumed to be 800 kg.

This implementation of the NASA Standard Breakup Model generates between 239 and 246 particles per run, with an average ejection velocity that is typically around around 70 m/s. The initial position and the initial velocities of all

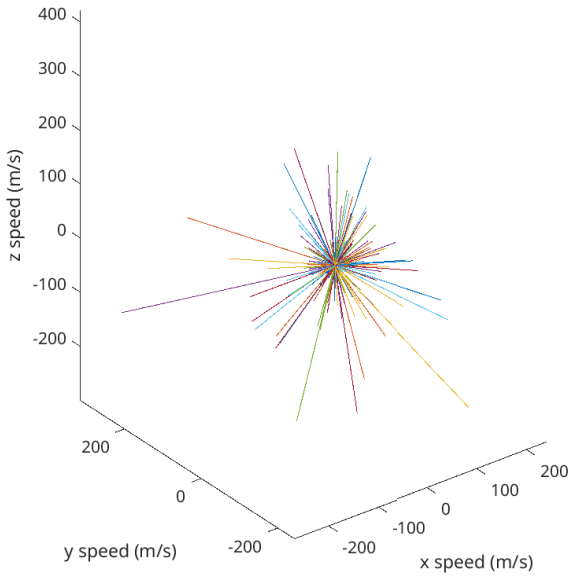

Fig. 2: Sample Ejection Velocity Vectors Generated by NASA Breakup Model

particles were used as the input for the orbit propagation. The cross-sectional area and mass of each particle was also used for the solar radiation pressure calculation in Eq. (4).

2.3 Monte Carlo Simulation Setup

The longevity of debris in lunar orbit following a spacecraft breakup event depends on a large number of uncertain variables, including the properties of the breakup event, where and when the breakup event occurs, and the initial pre-breakup orbit. Therefore, Monte Carlo simulations were used to randomly sample these variables. The resulting debris trajectories were propagated for each random sample, and then the results were aggregated to gain insight into the general behavior of debris in lunar orbit.

Six types of debris simulations were conducted to study how pre-breakup orbit inclination and altitude affects the longevity of debris in lunar orbit. Polar and retrograde equatorial circular orbits were considered with altitudes of 50 km, 100 km, and 200 km. These orbits were selected because they were used by several historical lunar spacecraft, as demonstrated in Table 1. A total of 50 runs were conducted for each of the six simulations, and each run began with random breakup event. The location of the breakup along the initial orbit, the breakup date and time, and the breakup properties were all randomly selected. Parameters fixed across all runs of a given simulation included the initial pre-breakup inclination, eccentricity, and altitude. The length of all runs was also fixed at 365 days. A summary of the parameters used for each run is provided in Table 2. The random initial pre-breakup orbits for the Polar 100 km debris simulation are plotted in Fig. 3.

The main result of each run was a list of the final states of all debris particles at the end of the 365-day propagation, including the time and location of lunar impact for particles that impacted the Moon. These lists could be aggregated across all runs to analyze the rate at which particles tended to decay to the lunar surface and identify patterns in where particles impacted the lunar surface. Six simulations of 50 runs each involved the propagation of a total of approximately 73,000 particles for one year. This involved substantial computational effort, necessitating the use of High Performance Computing (HPC). Simulation runs and the numerical integration of all particles in each run were accomplished in parallel using HPC resources.

Table 1: Simulations Conducted, with Relevant Lunar Missions

Simulation	Past Lunar Missions
Polar 50 km	GRAIL [17] LRO [18]
Polar 100 km	Chang'E-1 second orbit [19] Chang'E-2 [20] Chandrayaan-1 main mission orbit [21] Chandrayaan-2 [22] SELENE [23] Lunar Prospector [24]
Polar 200 km	Chang'E-1 initial orbit [19] Chandrayaan-1 initial orbit [21]
Retrograde Equatorial 50 km	None, for comparison only
Retrograde Equatorial 100 km	Apollo missions [4]
Retrograde Equatorial 200 km	None, for comparison only

Table 2: Selection of Parameters for Each Run

Parameter	Value
Run Length	Fixed at 365 days
Run Start Date/Time	Random between 1 Jan 2035 00:00:00 and 1 Jan 2036 00:00:00
Pre-Breakup Orbit Eccentricity	Fixed at zero (circular orbits)
Pre-Breakup Orbit Inclination	Fixed at 90 degrees (for polar simulations) or 180 degrees (for retrograde equatorial simulations)
Pre-Breakup Orbit Altitude	Fixed at 50 km, 100 km, or 200 km
Pre-Breakup Orbit Longitude of the Ascending Node	For polar cases, random between 0 and 360 degrees (not defined for retrograde equatorial cases)
Pre-Breakup Orbit Argument of Latitude	For polar cases, random between 0 and 360 degrees (not defined for retrograde equatorial cases)
Pre-Breakup Orbit True Longitude	For retrograde equatorial cases, random between 0 and 360 degrees (not defined for polar cases)
Breakup Properties	Randomly generated by NASA Standard Breakup Model

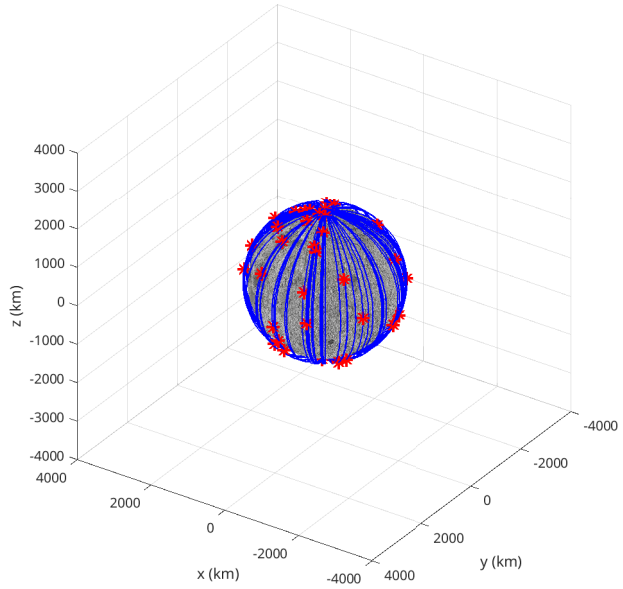

Fig. 3: Pre-Breakup Orbits for 100 km Polar Debris Simulation, with Breakup Locations Marked

2.4 Collision Probability Calculation

An estimation of the probability of collision with debris for other spacecraft operating in lunar orbit was also calculated for each of the six debris simulations. A technique similar to the Weibull distribution method described by Vedder and Tabor [25] and McCormick [26] was used to calculate the risk probability. In this method, miss distances between some notional spacecraft and the nearest debris object are generated, either through propagation or by randomly varying mean anomaly, and then a Weibull probability distribution function is fit to the miss distance measurements. The Weibull distribution is then used to infer the probability that a particle would pass close enough to the spacecraft to strike it. This method is a natural fit for the data generated by the Monte Carlo simulations described in Section 2.3. McCormick [26] also notes that this method only requires the orbit propagator to model the population of close approaches, and not to precisely predict all close approaches, relaxing the precision required for the orbit propagator.

In this study, the miss distance data was generated using the propagated debris trajectories. For each run, the absolute closest approach to any debris particle during the one-year propagation was tracked for two sets of randomly generated notional spacecraft (NSC). The two sets of spacecraft included 20 spacecraft initially at random positions along circular 100 km polar orbits with random longitude of the ascending node and 20 spacecraft initially at random positions along a circular 100 km retrograde equatorial orbit. The NSC were assumed to remain in unchanging orbits throughout the debris simulation, so they were propagated using a two-body force model. The NSC initial positions were randomly re-generated with each run. The locations of all randomly generated notional spacecraft for the Polar 100 km debris simulation are plotted in Fig. 4. Each simulation consisted of 50 runs, so 20 miss distance samples per run resulted in 1,000 miss distance samples for each notional spacecraft type. MATLAB's "fitdist" function was then used to fit a Weibull distribution to the miss distance data. The diameter of the spacecraft was assumed to be 1 m, so the probability that any particle would pass within 0.5 m of the spacecraft was inferred from the Weibull distribution.

3. RESULTS

The main results of this research effort include an analysis of the rate at which particles decayed to the lunar surface for each simulation, the distribution of impacts on the lunar surface, and the risk probabilities to other spacecraft operating in lunar orbit. These results are discussed in the following sections.

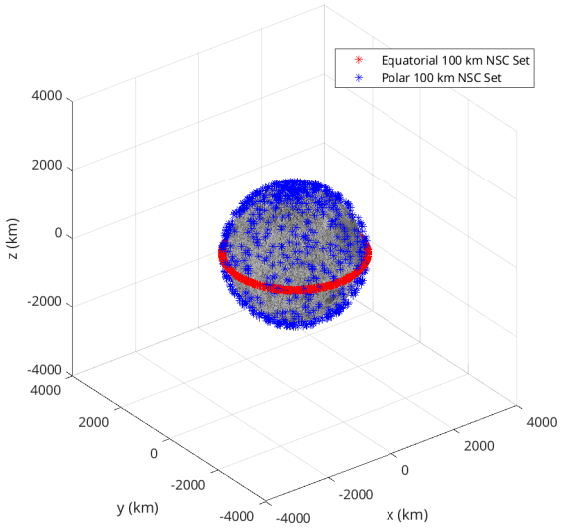

Fig. 4: Notional Spacecraft Initial Locations for Polar 100 km Simulation

3.1 Debris Decay Analysis

Fig. 5 shows the decay of particles from lunar orbit for each of the six simulations. Each line represents a run, i.e., a randomly generated breakup event. The distribution of the fraction of particles remaining after one year is also summarized with box plots in Fig. 6. Both the altitude at which the breakup event occurred and the initial orbit type greatly influenced the rate at which the debris decayed to the lunar surface. At least 60% of the particles generated by the breakup event had impacted the lunar surface after one year for all runs of the Polar 50 km, Retrograde Equatorial 50 km, and Polar 100 km simulations. However, most particles remained in lunar orbit after one year for the Retograde Equatorial 100 km, Polar 200 km, and Retrograde Equatorial 200 km simulations.

The relationship between the breakup altitude and the number of particles that had decayed within one year is expected due to the initial distance to the Moon's surface and differences in the effect of the non-spherical lunar gravity field by altitude. The non-spherical lunar gravity field is by far the largest perturbation causing objects in low lunar orbit to decay to the lunar surface [7], and this perturbation increases closer to the Moon. The particles in the 50 km cases decay quickly because they have initially low perilunes and are strongly perturbed by the lunar gravity field.

The slow rate of decay observed for the retrograde equatorial simulations is consistent with the remarkable stability of these orbits observed by Meador [4]. At least 75% of the particles remained in lunar orbit after one year in all runs of the Retrograde Equatorial 200 km simulation. Even in the Retrograde Equatorial 50 km simulation, few particles decayed from 150 to 365 days after the mishap. It seems likely that the particles remaining in the retrograde equatorial simulations have entered stable orbits and could remain in lunar orbit for years, much like the theorized fate of the Apollo 11 Lunar Module Ascent Stage.

The polar simulations in Fig. 5 exhibit an S-shaped shape, with decay rates that are initially low, increase after some time, and then decrease again. Note that the 100 km test orbit shown in Fig. 1a decayed after approximately 203 days, which is where the steepest rate of decay occurred in the Polar 100 km debris simulation, as shown in Fig. 5c. This suggests that the time for the debris particles to decay after the breakup event is related to the time it would have taken for the initial pre-breakup orbit to decay, as one might expect. Based on this observation, the Polar 200 km simulation likely would not have observed substantially more lunar impacts even if it had been extended to 1,000 days, because a polar 200 km orbit simulated in GMAT did not decay during this time. The slow decay rates at the end of the simulations may represent particles that have achieved stable or mostly stable orbits. It is unknown if this slow rate of decay would continue indefinitely or if it would eventually speed up again. Further analysis of the orbits these particles have achieved and the mechanism of their stability would be needed to make this determination.

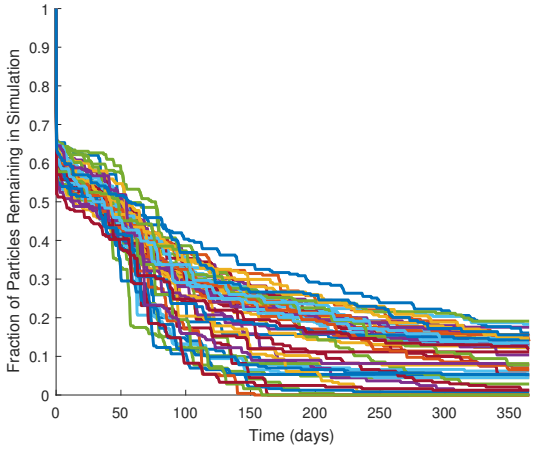

(a) Polar 50 km Simulation

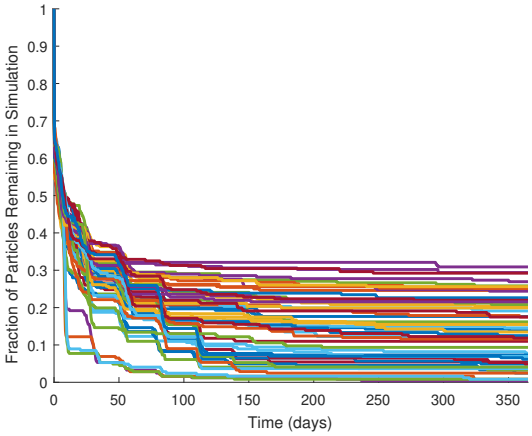

(b) Retrograde Equatorial 50 km Simulation

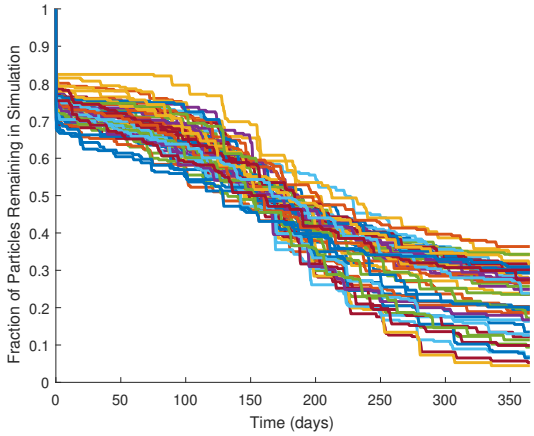

(c) Polar 100 km Simulation

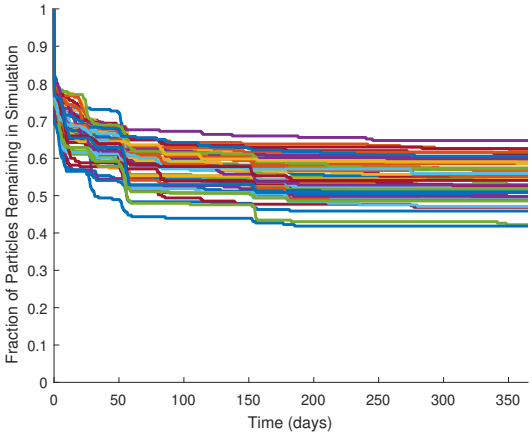

(d) Retrograde Equatorial 100 km Simulation

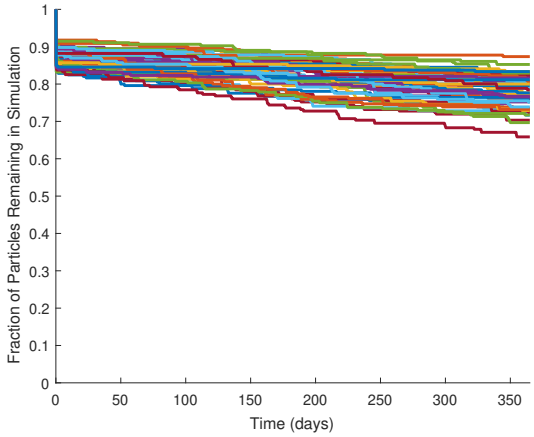

(e) Polar 200 km Simulation

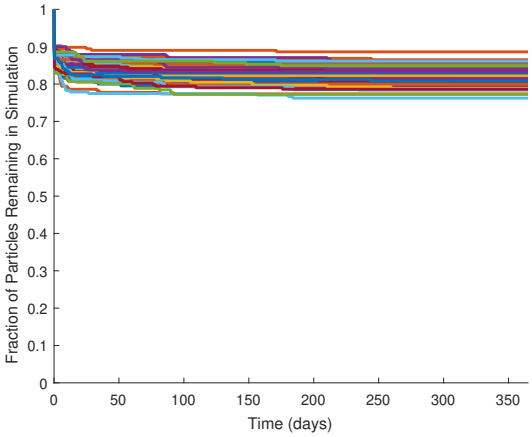

(f) Retrograde Equatorial 200 km Simulation

Fig. 5: Number of Particles Remaining in Each Simulation Run Over Time

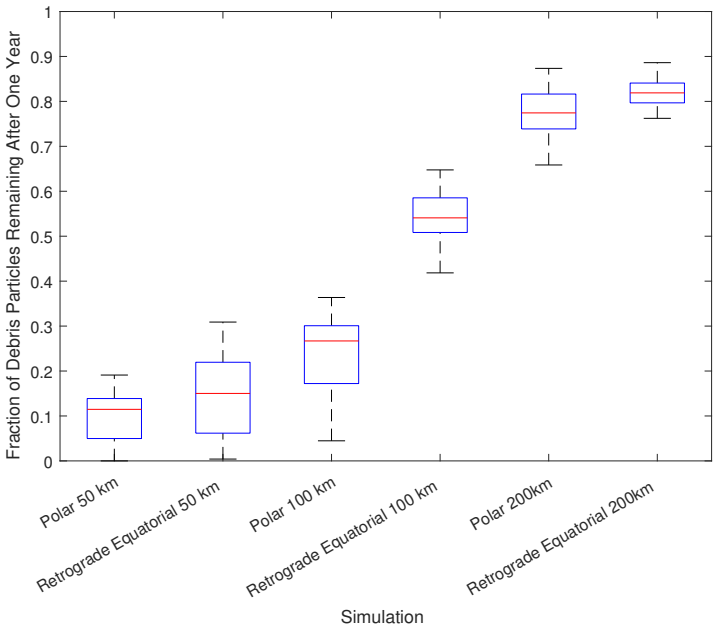

Fig. 6: Box Plot Summarizing Statistics for Fraction of Particles Remaining After One Year

3.2 Lunar Surface Impacts

The lunar surface impact locations are mapped for the Retrograde Equatorial 100 km simulation in Fig. 7a and for the Polar 100 km simulation in Fig. 7b. The Polar 100 km impacts at the north and south poles of the Moon are mapped in Fig. 8. The simulations at 50 km and 200 km had very similar surface impact locations, but with more impacts for the 50 km cases and fewer for the 200 km cases.

The Retrograde Equatorial 100 km simulation resulted in a line of impacts along the lunar equator, as expected because the initial pre-breakup lunar orbit only passed over the equator. There were few significant outliers and no obvious debris accumulations. The surface impacts for the Polar 100 km case were much more widely dispersed over the surface of the Moon, with some surprising accumulations of debris impacts at certain locations. Accumulations at the same locations were also observed in the 50 km and 200 km polar simulations. The most significant accumulation of impacts was between -90 to 0 degrees latitude and 50 to 90 degrees longitude, but a variety of smaller accumulations are visible.

It is not obvious why debris has accumulated at these locations, but this is almost certainly a result of the interaction between the debris and the non-spherical lunar gravity field. Certain topographical features of the Moon may cause a significant reduction in perilune when the Moon rotates such that those features are below a particle's orbit. If this were the case, one would expect to see relatively more impacts at a frequency that is in resonance with the lunar rotational frequency. Indeed, many of the plots in Fig. 5 do show a step-like behavior, with the steps often occurring at 14 or 28-day increments. Precession of the argument of perilune due to the lunar gravity field, much like the Earth's J2 effect, could also explain the some of the asymmetry in the distribution of impacts.

The distribution of impacts in Fig. 7b could have implications for end-of-life disposal of lunar spacecraft. Johnson [2] suggested that certain locations on the Moon could be designated as "satellite dumping grounds," and the regions with significant impacts observed in Fig. 7b could be ideal for this purpose. This is because the natural tendency of debris to strike these locations could reduce the fuel cost required to reach them, meaning that spacecraft would need to budget less fuel for targeted disposal on the lunar surface, thus extending their operational lifetimes. Furthermore, designation of these areas as lunar dumping grounds would ensure that the areas that would be most at risk from impacts following an orbital breakup event would be clear of crewed settlement or important infrastructure. Further research is needed to explore the viability of these locations as lunar satellite dumping grounds.

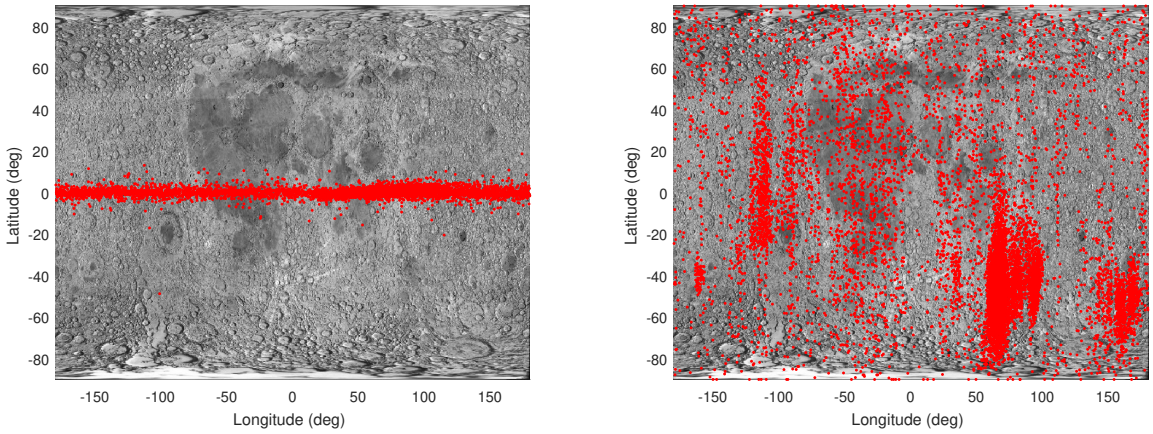

(a) Retrograde Equatorial 100 km Simulation

(b) Polar 100 km Simulation

Fig. 7: Lunar Surface Impacts

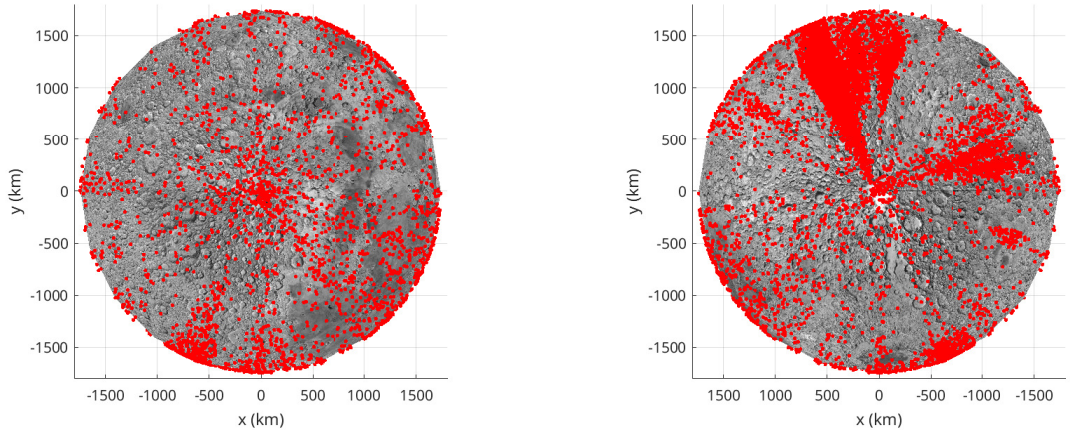

(a) North Pole Surface Impacts

(b) South Pole Surface Impacts

Fig. 8: Impacts at Lunar Poles, Polar 100 km Simulation

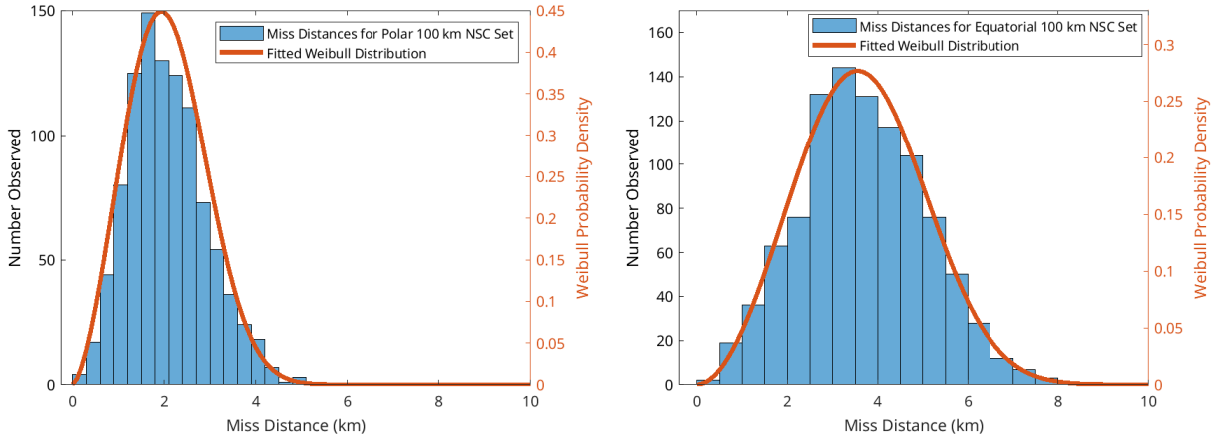

(a) Polar 100 km Notional Spacecraft Set

(b) Equatorial 100 km Notional Spacecraft Set

Fig. 9: Distribution of Notional Spacecraft Miss Distances, Polar 100 km Simulation

Table 3: Probability of Collision Results

Case	Polar 100 km NSC Set	Retrograde Equatorial 100 km NSC Set
Polar 50 km	1.33×10^{-9}	6.33×10^{-13}
Polar 100 km	2.65×10^{-10}	4.74×10^{-12}
Polar 200 km	3.16×10^{-10}	2.04×10^{-12}
Retrograde Equatorial 50 km	2.01×10^{-12}	1.44×10^{-10}
Retrograde Equatorial 100 km	2.80×10^{-12}	9.27×10^{-10}
Retrograde Equatorial 200 km	2.30×10^{-13}	2.50×10^{-10}

3.3 Collision Probability

For each of the six simulations, the absolute closest approaches over the one-year propagation window to two different types of randomly generated notional spacecraft were calculated according to the procedure discussed in Section 2.4. The Weibull distribution was an excellent fit for the miss distance data, as shown for the Polar 100 km simulation Fig. 9. The probabilities of collision for the two types of notional spacecraft are shown in Table 3. The risk probability varied between 10^{-9} and 10^{-13} depending on the breakup orbit and the orbit type of the notional spacecraft.

As expected, the probability of collision was the highest when the debris event orbit type matched the orbit type of the notional spacecraft. The Retrograde Equatorial 100 km debris events posed the greatest threat to Retrograde Equatorial 100 km spacecraft, while the Polar 50 km debris event posed the greatest threat to the Polar 100 km spacecraft. It is not clear why the Polar 50 km debris event resulted in the highest probability of collision to the Polar 100 km notional spacecraft. This could be statistical noise, or it may be related to the breakups leading to a significant number of particles with apolunes at or greater than 100 km such that they would pass through the 100 km altitude level as they decayed.

4. CONCLUSION

This study examined the effects of significant debris-generating events in lunar orbit. Using a high-precision orbit propagator coupled with Monte Carlo simulation, insight was gained into the time required for debris to decay from orbit, the locations of debris impacts on the Moon, and the collision risk to other lunar spacecraft. Debris simulations were conducted in polar and retrograde equatorial lunar orbits at 50 km, 100 km, and 200 km altitude to compare the

effects of breakup altitude and orbit type on the propagation of debris.

The altitude and initial orbit type both strongly influenced the propagation of debris. Debris in retrograde equatorial orbits generally took longer to decay than polar orbits, and as much as 90% of the debris remained in lunar orbit after one year for both orbit types at 200 km altitude. These results suggest that particular importance should be placed on disposal of lunar spacecraft operating in retrograde equatorial orbits at an altitude of 100 km or higher and polar orbiting spacecraft operating at 200 km or higher. At least some debris remained in lunar orbit after one year for nearly all of the breakup simulations, with some indications that these objects could be stable in orbit for much longer than one year. Further research is needed to determine the mechanism of their stability and how long these particles would remain in orbit.

The analysis of surface impact locations for the polar breakup scenarios showed a surprising degree of asymmetry in the locations of surface impacts, with significant accumulations at certain regions of the Moon. Threats to lunar surface infrastructure in these regions could be a concern. These locations could also be optimal locations for a designated lunar spacecraft disposal site in the future, but further research is needed to evaluate their viability for this purpose.

Finally, the probability of collision with other notional polar and retrograde equatorial spacecraft varied between 10^{-13} and 10^{-9} over one year, depending on the breakup orbit and the notional spacecraft orbit. This indicates a low risk of collision. However, the large number of observed close approaches within 5 km may generate some concern, especially considering the difficulties tracking objects so far from Earth.

This research could be extended in the future through debris simulations in other orbit types and for longer time windows. Analysis of breakup events in lunar frozen orbits, which are low lunar orbits with known stability, would be useful to determine if the debris is also stable in these orbits. Orbits with planned use for crewed lunar exploration, such as the Lunar Gateway's Near Rectilinear Halo Orbit, would also be useful for debris analysis to understand the possible risk to humans. A thorough evaluation of the risks of debris in lunar orbit is especially important as crewed exploration of the Moon resumes, providing assessments of the overall hazard level and emphasizing the importance of proper lunar spacecraft disposal.

5. REFERENCES

[1] Donald J. Kessler and Burton J. Cour-Palais. Collision frequency of artificial satellites: The creation of a debris belt. *Journal of Geophysical Research*, 83(A6):2637–2646, 1978.

[2] Nicholas L. Johnson. Man-made debris in and from lunar orbit. In *50th International Astronautical Congress Proceedings*, 1999.

[3] Nathan R. Boone and Robert A. Bettinger. Artificial debris collision risk following a catastrophic spacecraft mishap in lunar orbit. In *2021 Advanced Maui Optical Surveillance Conference (AMOS) Proceedings*, 2021.

[4] James Meador. Long-term orbit stability of the Apollo 11 "Eagle" lunar module ascent stage. *Planetary and Space Science*, 205, 2021.

[5] Steve Hughes. General Mission Analysis Tool (GMAT) technical specifications. NASA Technical Reports Server (1 Jan 2007).

[6] National Aeronautics and Space Administration. A standardized lunar coordinate system for the Lunar Reconnaissance Orbiter and lunar datasets. Available at https://lunar.gsfc.nasa.gov/library/LunCoordWhitePaper-10-08.pdf (1 Oct 2008).

[7] Young-Joo Song, Sang-Young Park, Hae-Dong Kim, and Eun-Sup Sim. Development of precise lunar orbit propagator and lunar polar orbiter's lifetime analysis. *Journal of Astronomy and Space Sciences*, 27(2):97–106, 2010.

[8] William M. Folkner, James G. Williams, and Dale H. Boggs. The planetary and lunar ephemeris DE 421. IPN Progress Report 42-178, 15 Aug 2009.

[9] National Aeronautics and Space Administration. Lunar gravity field: GRGM1200A. Available at https://pgda.gsfc.nasa.gov/products/50.

[10] Richard H. Battin. *An Introduction to the Mathematics and Methods of Astrodynamics, Revised Edition*. American Institute of Aeronautics and Astronautics, 1999.

[11] David A. Vallado. *Fundamentals of Astrodynamics and Applications*. Microcosm Press, 2007.

[12] Oliver Montenbruck. *Satellite Orbits: Models, Methods, Applications*. Springer, 2000.

[13] N.L. Johnson, P.H. Krisko, J.-C. Liou, and P.D. Anz-Meador. NASA's new breakup model of EVOLVE 4.0. *Advances in Space Research*, 28(9):1377–1384, 2001.
[14] Stefan Frey and Camilla Colombo. Transformation of satellite breakup distribution for probabilistic orbital collision hazard analysis. *Journal of Guidance, Control, and Dynamics*, 44(1):88–105, 2021.
[15] Paula H. Krisko. Proper implementation of the 1998 NASA breakup model. *Orbital Debris Quarterly News*, 15(4):4–5, 2011.
[16] Eric W. Weisstein. Sphere point picking. https://mathworld.wolfram.com/SpherePointPicking.html.
[17] D.H. Lehman, T.L. Hoffman, and G.G. Havens. The Gravity Recovery and Interior Laboratory mission. In *2013 IEEE Aerospace Conference Proceedings*, March 2013.
[18] Richard Vondrak, John Keller, and James Garvin. Lunar Reconnaissance Orbiter (LRO): Observations for lunar exploration and science. *Space Science Reviews*, 150:391–419, 2010.
[19] X.-D. Wang, W. Bian, J.-S. Wang, J.-J. Liu, Y.-L. Zou, H.-B. Zhang, C. Lü, J.-Z. Liu, W. Zuo, Y. Su, W.-B. Wen, M. Wang, Z.-Y. Ouyang, and C.-L. Li. Acceleration of scattered solar wind protons at the polar terminator of the Moon: Results from Chang'E-1/SWIDs. *Geophysical Research Letters*, 37(7), 2010.
[20] PeiJia Li, XiaoGong Hu, Yong Huang, GuangLi Wang, DongRong Jiang, XiuZhong Zhang, JianFeng Cao, and Nan Xin. Orbit determination for Chang'E-2 lunar probe and evaluation of lunar gravity models. *Science China Physics, Mechanics and Astronomy*, 55:514–522, 2012.
[21] Jitendra Nath Goswami and Mylswamy Annadurai. Chandrayaan-1 mission to the moon. *Acta Astronautica*, 63(11):1215–1220, 2008.
[22] Venkatesan Sundararajan. Overview and technical architecture of india's Chandrayaan-2 mission to the Moon. In *2018 AIAA Aerospace Sciences Meeting*, 2018.
[23] M. Kato, S. Sasaki, K. Tanaka, Y. Iijima, and Y. Takizawa. The Japanese lunar mission SELENE: Science goals and present status. *Advances in Space Research*, 42(2):294–300, 2008.
[24] L. L. Hood, A. Zakharian, J. Halekas, D. L. Mitchell, R. P. Lin, M. H. Acuña, and A. B. Binder. Initial mapping and interpretation of lunar crustal magnetic anomalies using Lunar Prospector magnetometer data. *Journal of Geophysical Research: Planets*, 106(E11):27825–27839, 2001.
[25] John D. Vedder and Jill L. Tabor. New method for estimating low-earth-orbit collision probabilities. *Journal of Spacecraft and Rockets*, 28(2):210–215, 1991.
[26] Bernell McCormick. Collision probabilities in geosynchronous orbit and techniques to control the environment. *Advances in Space Research*, 6(7):119–126, 1986.